CRYSTAL GROWTH & DESIGN

pubs.acs.org/crystal

Article

Development of High-Quality SAM on Sapphire Pseudosubstrate by SPE for Long-Wavelength LEDs

Guangying Wang,* Shuwen Xie, Sam Oliyai, Surjava Sanyal, Moon J. Kim, and Shubhra Pasayat

Cite This: *Cryst. Growth Des.* 2024, 24, 9538−9543

Read Online

ACCESS | Metrics & More | Article Recommendations

ABSTRACT: One of the main challenges in achieving long-wavelength InGaN-based emitters is their large lattice mismatch, around 11% between InN and GaN. $ScAlMgO_4$ (SAM) is lattice-matched with $In_{0.17}Ga_{0.83}N$, which allows the growth of high indium composition InGaN films with good quality. Using solid-phase epitaxy (SPE) of SAM on a sapphire substrate, SAM films can be achieved at any wafer size with greatly reduced cost while keeping their lattice-matched properties. In this work, we have achieved smooth InGaN films grown on SAM on sapphire with similar morphology as InGaN films deposited on free-standing native SAM substrates. Moreover, we have demonstrated the first InGaN-based green LED on SAM on a sapphire substrate with a peak emission wavelength at 525 nm and ∼9 nm of blue shift.

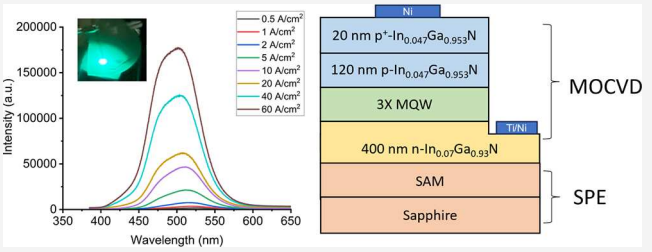

INTRODUCTION

III-Nitride materials have been favored for visible-range optical devices due to their high efficiency and stability.[1−4] Using GaN and InN, InGaN-based LEDs can cover the wavelength range from near UV to near IR[1]. Currently, GaN on Silicon or GaN on sapphire are commonly used as substrates or templates for InGaN-based devices. One of the main challenges of long wavelength InGaN-based LED is the large lattice mismatch between InN and GaN, which is around 11%.[5−8] This lattice mismatch will cause significant strain, leading to dislocations and the formation of crystal defects, which makes it challenging to achieve high indium content.[5] Therefore, developing a relaxed InGaN layer is essential for III-Nitride-based long-wavelength emitters. Different approaches to achieve a relaxed InGaN layer have been widely explored, such as creating a flexible underlayer with thermal decomposition of underlying high-composition InGaN[9−11] or porosification of Si-doped GaN.[12−14] These approaches have effectively demonstrated the relaxation of InGaN, resulting in a redshift in emission. However, thermal decomposition requires a high-composition InGaN layer, which may lead to high dislocation and defects. Additional fabrication steps are required to create porosified substrates before InGaN deposition.[11,14] Another way to achieve relaxed InGaN buffer layers is by using lattice-matched substrates, such as ZnO or $ScAlMgO_4$ (SAM). ZnO is lattice-matched to $In_{0.22}Ga_{0.78}N$. However, a very low deposition temperature (<600 °C) is required to prevent ZnO decomposition.[15−18] SAM is lattice-matched with $In_{0.17}Ga_{0.83}N$ and only 2% mismatched with GaN, which makes it a great candidate for the deposition of III-Nitride materials.[19−22] Recently, thick InGaN buffer layers along with red InGaN quantum well have been successfully demonstrated on bulk SAM substrates with step-flow morphology and red PL emission.[19,20] However, bulk SAM substrates are only available in small sizes and with high cost (>4000 $ for a 2-in. wafer),[23] which is quite limiting for extensive research and commercialization.

High-quality SAM on sapphire substrate can be created through SPE of amorphous SAM on sapphire followed by crystallization. This method allows SAM to be deposited on any size of a sapphire wafer while still maintaining low lattice mismatch with high-composition InGaN layers deposited on them. However, a key challenge with SPE of SAM is that the scandium-deficient regions may appear due to unoptimized crystallization conditions, leading to the formation of undesirable spinel-phase $MgAl_2O_4$ material with high surface roughness.[24,25] Recently, we have performed a systematic study of SAM crystallization with different annealing conditions and demonstrated a reduction in the spinel phase (spinel to SAM phase volumetric ratio decreased from 1 to 0.2) as well as up to 120 nm photoluminescence (PL) red-shift compared to the same film grown on GaN on sapphire.[24] However, the residual spinel phase still affected the surface morphology, and the surface roughness of SAM on sapphire (∼2 nm) was still

Received: July 17, 2024
Revised: October 23, 2024
Accepted: October 23, 2024
Published: October 31, 2024

https://doi.org/10.1021/acs.cgd.4c00990
Cryst. Growth Des. 2024, 24, 9538−9543

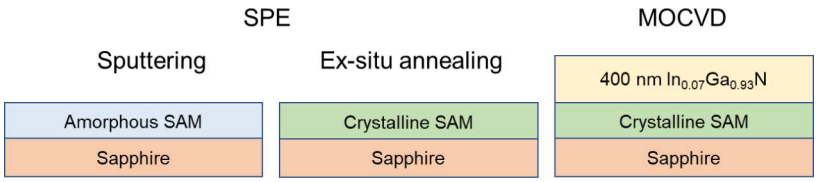

Figure 1. Illustration of MOCVD-grown InGaN deposited on SPE SAM on sapphire.

significantly higher than conventional substrates such as GaN on sapphire template (<0.2 nm), leading to a high surface roughness of InGaN buffer layers deposited above these SAM on sapphire pseudosubstrates.[24]

In this work, we have further improved the sputtering condition of SAM and, consequently, the InGaN material quality deposited on SAM on sapphire pseudosubstrates. The spinel phase was suppressed to minimal intensity, and low surface roughness similar to a conventional bulk SAM substrate (RMS ∼ 0.3 nm) was achieved on SAM on sapphire.[23] The Metal−Organic Chemical Vapor Deposition (MOCVD) grown InGaN on SAM on sapphire demonstrated similar roughness as the InGaN grown on bulk SAM substrates. InGaN-based green LED structure was deposited on SAM on a sapphire substrate, resulting in an emission wavelength of 525 nm at 0.5 A/cm^2. These results demonstrate the potential of using SPE of SAM for long wavelength emitters.

METHOD

The amorphous SAM film was deposited on a sapphire (Al_2O_3) substrate with pretreatment through the RF sputtering method using the Denton Discovery 24 tool. Details of sapphire pretreatment were described in the previous work.[24] The sputtering condition included a 100 W RF power, 10 mTorr chamber pressure, and 10 sccm Argon flow. Thereafter, the film was transferred to a high-temperature furnace and annealed at different temperatures, 775 °C, 825 °C, 875 and 950 °C, for 10 h in air under atmosphere pressure. After the crystallization process, the wafers were loaded into the MOCVD chamber for the deposition of the InGaN film (Figure 1). The precursors used during the MOCVD deposition included triethylgallium (TEGa) and trimethylindium (TMI) for the group III species, and ammonia (NH_3) for the group V species. A 400 nm thick InGaN film was deposited at 920 °C.[26,27] InGaN (or Indium content) calibration was first performed on standard GaN on a sapphire substrate, and no strain relaxation methods were employed. Based on our calibration and past PL studies, the expected Indium content was ∼7% and ∼14% when the same deposition parameters were used on GaN on sapphire and SAM on sapphire, respectively.[24] The RMS surface roughness was obtained on both amorphous and crystalline SAM on sapphire samples with Atomic Force Microscopy (AFM) by using a Bruker Icon AFM tool. X-ray diffraction (XRD) was performed on SAM on sapphire for crystallinity using an XRD Panalytical Empyrean tool. Scanning Transmission Electron Microscopy (S-TEM) was performed to examine the SAM and sapphire interface. After examining the surface morphology and crystallinity of the underlayers, SAM on sapphire samples showed reasonable results as a substrate for III−N-based LED devices. Therefore, an InGaN-based LED structure was deposited above these SAMs on sapphire substrates with an InGaN buffer layer.

The LED structure involved 400 nm of Si-doped $In_{0.07}Ga_{0.93}N$ deposited at 920 °C with GaN interlayers, 3 repetition of multiple quantum wells (MQW) comprising of 2.7 nm InGaN quantum well (QW), 1.5 nm AlGaN QW cap and 10 nm GaN quantum barrier (QB), 120 nm of Mg-doped $In_{0.045}Ga_{0.955}N$ layer and a 20 nm of heavily p-doped $In_{0.045}Ga_{0.955}N$ grown at 940 °C. The InGaN QW and cap were deposited at 800 °C, and the GaN QB was deposited at 900 °C. The pressure was kept at 375 Torr throughout the deposition, and the NH_3 flow was kept at 178.5 mmol min^{-1} for the InGaN layers. The LED activation was performed at 600 °C for 20 min in air ambient. 50 × 50 μm^2 devices were defined through optical lithography patterning (Heidelberg DWL 66+ laser writer) followed by a low power (15 W) reactive ion etch (RIE) pattern etching with chlorine gas to reduce sidewall damage. The metal stack of 30 nm/250 nm Ti/Ni and 70 nm Ni was deposited as n-contact and p-contact, respectively, by using an E-beam evaporator.

RESULT

In this experiment, 30 nm of amorphous SAM on sapphire was annealed at temperatures ranging from 775 to 950 °C for 10 h in air. All the wafers underwent a preannealing step to assist crystallization, which was discussed in our previous study.[24] Annealing temperatures were varied to find the optimal balance of crystallization and roughness. The higher annealing temperature may accelerate the crystallization process of the amorphous film due to the presence of thermal energy. However, a higher temperature may also lead to a larger grain size, leading to the film's roughness.[28−31] In the case of SAM on sapphire, a high annealing temperature will also promote the formation of undesired $MgAl_2O_4$ spinel phase, resulting in high surface roughness and uneven stoichiometry. Therefore, finding the optimized temperature to ensure crystallization while minimizing the surface roughness is essential for achieving high-quality SAM on sapphire. The annealing temperature of SAM on sapphire was first set to 950 °C to ensure crystallization. The XRD omega-2-theta scan showed a minimal spinel peak ($MgAl_2O_4$) with all annealing temperatures (Figure 2). With the annealing temperature changed from 950 to 825 °C, although the XRD scans' background noise was different, the peak intensity among different samples is very similar, indicating the films were fully crystallized. However, as the annealing temperature decreased from 825 to 775 °C, the intensity of the SAM 009 peak was barely visible, leaving only the substrate sapphire peak the dominant peak. This behavior showed that a low volume of crystalline material was detected, indicating the film was likely not fully crystallized, which is at the partial-crystallization stage.

The RMS roughness of amorphous SAM on sapphire in a 1 × 1 μm^2 scan size was 0.214 nm (Figure 3a). A surface roughness of 0.982 nm (Figure 3b) was achieved with a 950 °C crystallization temperature, which is around four times higher than amorphous SAM on sapphire (Figure 3a). When the annealing temperature was decreased to 775 °C, the roughness of crystalline SAM on sapphire decreased to 0.21

https://doi.org/10.1021/acs.cgd.4c00990
Cryst. Growth Des. 2024, 24, 9538−9543

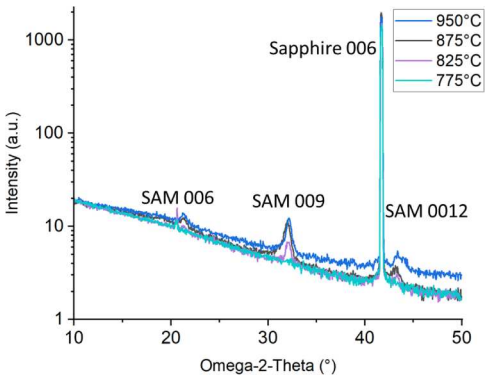

Figure 2. XRD omega-2-theta scan of SAM on sapphire with various temperatures.

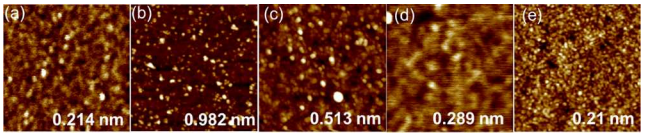

Figure 3. AFM scan with 1 × 1 μm^2 scan size of SAM on sapphire samples: (a) as-deposited amorphous film, (b) with 950 °C annealing temperature, (c) with 875 °C annealing temperature, (d) with 825 °C annealing temperature, and (e) with 775 °C annealing temperature.

nm, which is very similar to the amorphous SAM on sapphire substrate. While comparing the surface morphology of the two samples in the 3D AFM image, the grain sizes are smaller and more evenly distributed at 775 °C than 950 °C (Figure 4). The roughness of the crystalline SAM on sapphire was observed to be proportionate with the annealing temperature (Figure 3).

The result of the AFM scan of the sample annealed at 775 °C, which showed no roughness increment when compared with the amorphous sample, further confirmed the assumption drawn from the XRD result that the sample is likely at the partial-crystallization stage. A longer annealing time might be needed for samples with an annealing temperature of 775 °C to fully crystallize. Therefore, we believe an 825 °C annealing temperature for a duration of 10 h for a 30 nm thick SAM film on a sapphire substrate is the most optimal condition among all temperatures due to its low surface roughness and efficient crystallization process. The surface morphology and crystallinity improved significantly from our previous work. AFM roughness reduced from ∼1.25 nm to ∼0.3 nm, and the spinel to SAM phase volumetric ratio decreased from ∼0.2 to nearly 0.

Moreover, high-resolution scanning transmission electron microscopy (STEM) analysis was conducted at the interface (Figure 5). The area of interest (AOI) shows focuses on the

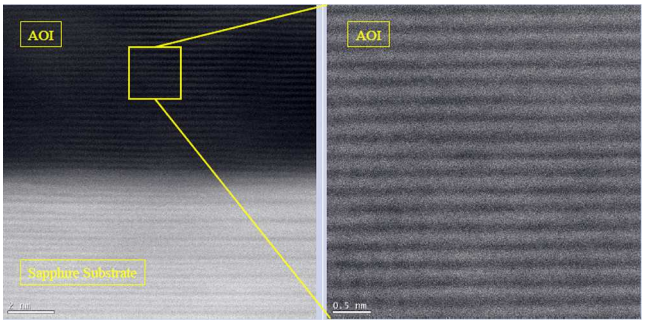

Figure 5. High-angle annular dark field (HAADF) STEM image showing SAM and sapphire layers.

SAM film, which exhibited a columnar structure, indicating crystallization. Organized columnar patterns in the crystalline region of the SAM film suggest low defect density. However, dark areas observed in the TEM scan indicate scattering losses, likely due to partial crystallization. These promising results indicated that the SAM on a sapphire substrate has the potential to achieve a quality similar to that of a bulk SAM substrate.

SAM layers on sapphire substrate crystallized at 825 °C were used for the MOCVD of InGaN layers due to their low roughness and crystalline properties. An AFM scan of 10 × 10 μm^2 was performed on both InGaN on SAM on sapphire (Figure 6a) and on a coloaded bare sapphire sample (Figure 6b). The only difference between the two samples was the 30 nm crystalline SAM layer, however, the film surface after the InGaN deposition demonstrated significantly improved surface roughness and morphology for the sample with the SAM layer. Lower surface roughness of 11.7 nm was achieved on SAM on the sapphire sample, while InGaN film deposited on the sapphire showed a roughness of 27.4 nm. Moreover, the InGaN film deposited on SAM on sapphire formed small

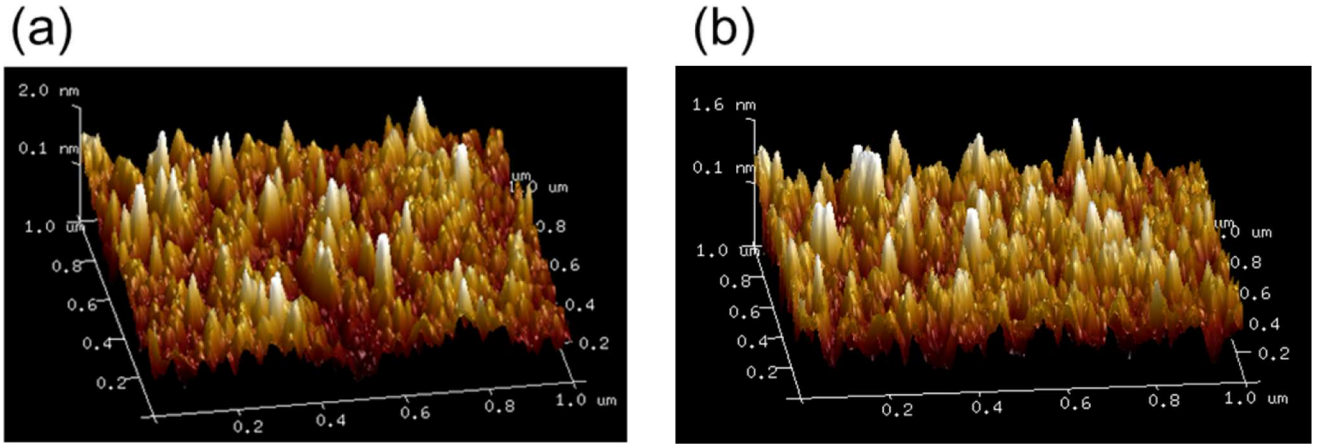

Figure 4. 3D AFM scan with 1 × 1 μm^2 scan size on crystalline SAM on sapphire samples with (a) 950 °C annealing temperature and 825 °C annealing temperature.

https://doi.org/10.1021/acs.cgd.4c00990
Cryst. Growth Des. 2024, 24, 9538−9543

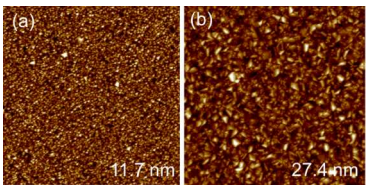

Figure 6. AFM scan of InGaN on (a) SAM on sapphire and (b) sapphire.

grains with uniform size and distribution. On the contrary, the InGaN film deposited directly on sapphire showed large facets with different orientations, indicating an undesirable 3-D island growth mode. Although the surface roughness of InGaN deposited on SAM on sapphire substrate is still relatively higher when compared to InGaN deposited on conventional GaN on sapphire samples, this roughness of 11.7 nm is very similar to the previous report of InGaN on native SAM substrates (10.7 nm in a 3× 3 μm^2 scan).[20] This surface morphology has been considered acceptable to proceed with InGaN-based QW and LED structure demonstrations on native SAM substrates by the community.[21,22] Therefore, our promising buffer morphology result encouraged us to proceed with device demonstration on SAM on the sapphire substrate. The green InGaN-based LED structure was deposited on the SAM on a sapphire substrate and coloaded sapphire substrate. The device was fabricated into 50 × 50 μm^2 sized micro-LED with a peak emission wavelength of 525 nm at 0.5 A/cm^2 on SAM on sapphire substrate (Figure 7). The same device grown on sapphire substrate did not light up at low current density (<5 A/cm^2) and showed extremely dim emission compared with device grown on SAM on sapphire. With increasing injection current density, the emission wavelength of SAM on sapphire showed a blue shift due to reduced quantum confined stark effect due to the flattened bandgap with higher bias application. From 5 A/cm^2 to 60 A/cm^2, the wavelength shifted by ∼9 nm, comparable to the state-of-the-art high-efficiency green micro-LEDs.[13] However, the fwhm of this device (∼80 nm) was much larger than the other green LEDs on GaN on the sapphire substrate at similar wavelengths (∼40 nm). This was possibly due to unoptimized LED growth conditions, resulting in indium segregation in the MQW. Moreover, the surface roughness of InGaN on SAM on sapphire is still relatively higher than InGaN on commercially used GaN on sapphire, which may further worsen the indium segregation. In future work, growth conditions will be further optimized to reduce the indium segregation effect and improve the fwhm of the emission peak.

CONCLUSION

In this work, we further improved both the crystallinity and the surface morphology of the SPE SAM film on the sapphire substrate. With a roughness of ∼0.3 nm and a spinel to SAM volumetric ratio of ∼0, we were able to achieve a smooth surface of MOCVD-grown InGaN film on SAM substrate, with surface roughness of ∼12 nm for InGaN buffer layers, nominally similar to that deposited on bulk SAM substrate. The Green LED structure deposited on SAM on sapphire substrate showed a peak emission wavelength of around 525 nm at 0.5 A/cm^2 and a similar blue shift (∼9 nm) compared to the state-of-the-art LEDs at a similar wavelength. Although the fwhm of the emission peak is much larger when compared to devices at similar wavelengths, this preliminary result showed great potential for using SAM on sapphire substrate for long wavelength emitters.

ASSOCIATED CONTENT

Data Availability Statement

The data that support the findings of this study are available from the corresponding authors upon reasonable request.

AUTHOR INFORMATION

Corresponding Author

Guangying Wang − *Department of Electrical and Computer Engineering, University of Wisconsin−Madison, Madison, Wisconsin 53706, United States;* orcid.org/0000-0002-4278-3037; Email: gwang265@wisc.edu

Authors

Shuwen Xie − *Department of Electrical and Computer Engineering, University of Wisconsin−Madison, Madison, Wisconsin 53706, United States*

Sam Oliyai − *Department of Materials Science and Engineering, The University of Texas at Dallas, Richardson, Texas 75080, United States*

Surjava Sanyal − *Department of Electrical and Computer Engineering, University of Wisconsin−Madison, Madison, Wisconsin 53706, United States*

Moon J. Kim − *Department of Materials Science and Engineering, The University of Texas at Dallas, Richardson,*

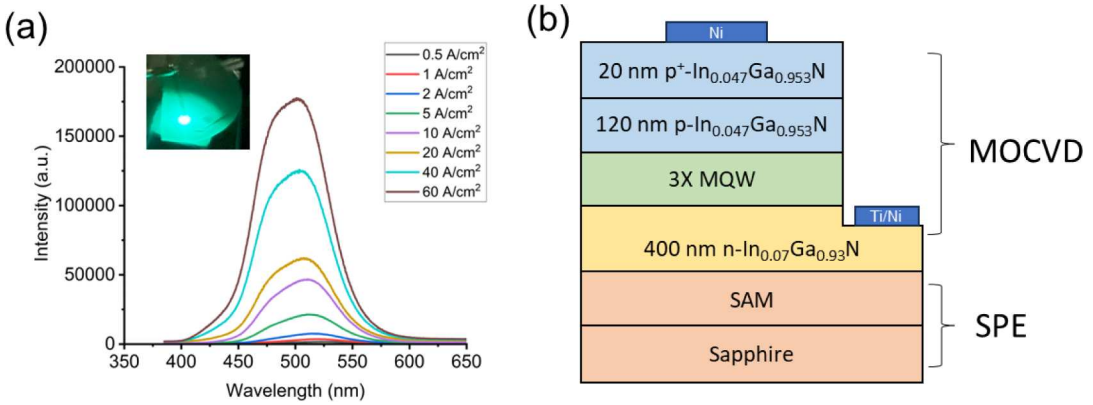

Figure 7. Electroluminescence of InGaN-based LED on SAM on sapphire with an injection current of 0.5 A/cm^2 to 60 A/cm^2 with emission optical image at 2 A/cm^2.

https://doi.org/10.1021/acs.cgd.4c00990
Cryst. Growth Des. 2024, 24, 9538−9543

Texas 75080, United States; orcid.org/0000-0002-2972-493X

Shubhra Pasayat − *Department of Electrical and Computer Engineering, University of Wisconsin−Madison, Madison, Wisconsin 53706, United States*

Complete contact information is available at: https://pubs.acs.org/10.1021/acs.cgd.4c00990

Funding

This work was supported partially by the National Science Foundation under Grant ECCS-2338683 and partially by the Office of Naval Research under Grant N00014-22-1-2267 and monitored by Paul Maki.

Notes

The authors declare no competing financial interest.

REFERENCES

(1) Kour, R.; Arya, S.; Verma, S.; Singh, A.; Mahajan, P.; Khosla, A. Review—Recent Advances and Challenges in Indium Gallium Nitride (InxGa1-xN) Materials for Solid State Lighting. *ECS J. Solid State Sci. Technol.* **2020**, *9* (1), 015011.

(2) Buffolo, M.; Caria, A.; Piva, F.; Roccato, N.; Casu, C.; De Santi, C.; Trivellin, N.; Meneghesso, G.; Zanoni, E.; Meneghini, M. Defects and Reliability of GaN-Based LEDs: Review and Perspectives. *Phys. Status Solidi A* **2022**, *219* (8), 2100727.

(3) Li, P.; Li, H.; Wong, M. S.; Chan, P.; Yang, Y.; Zhang, H.; Iza, M.; Speck, J. S.; Nakamura, S.; Denbaars, S. P. Progress of InGaN-Based Red Micro-Light Emitting Diodes. *Crystals* **2022**, *12* (4), 541.

(4) Lu, Z.; Zhang, K.; Zhuang, J.; Lin, J.; Lu, Z.; Jiang, Z.; Lu, Y.; Chen, Z.; Guo, W. Recent Progress of InGaN-Based Red Light Emitting Diodes. *Micro Nanostruct.* **2023**, *183*, 207669.

(5) Langer, T.; Kruse, A.; Ketzer, F. A.; Schwiegel, A.; Hoffmann, L.; Jönen, H.; Bremers, H.; Rossow, U.; Hangleiter, A. Origin of the "Green Gap": Increasing Nonradiative Recombination in Indium-Rich GaInN/GaN Quantum Well Structures. *Phys. Status Solidi C* **2011**, *8* (7−8), 2170−2172.

(6) Rinke, P.; Scheffler, M.; Qteish, A.; Winkelnkemper, M.; Bimberg, D.; Neugebauer, J. Band Gap and Band Parameters of InN and GaN from Quasiparticle Energy Calculations Based on Exact-Exchange Density-Functional Theory. *Appl. Phys. Lett.* **2006**, *89* (16), 161919.

(7) Kim, Y. H.; Park, H. J.; Kim, K.; Kim, C. S.; Yun, W. S.; Lee, J. W.; Kim, M. D. Strain Distribution and Interface Modulation of Highly Lattice-Mismatched InN/GaN Heterostructure Nanowires. *Appl. Phys. Lett.* **2009**, *95* (3), 033112.

(8) Yamaguchi, S.; Kariya, M.; Nitta, S.; Takeuchi, T.; Wetzel, C.; Amano, H.; Akasaki, I. Structural Properties of InN on GaN Grown by Metalorganic Vapor-Phase Epitaxy. *J. Appl. Phys.* **1999**, *85* (11), 7682−7688.

(9) Chan, P.; DenBaars, S. P.; Nakamura, S. Growth of Highly Relaxed InGaN Pseudo-Substrates over Full 2-in. *Appl. Phys. Lett.* **2021**, *119* (13), 131106.

(10) Wong, M. S.; Chan, P.; Lim, N.; Zhang, H.; White, R. C.; Speck, J. S.; Denbaars, S. P.; Nakamura, S. Low Forward Voltage III-Nitride Red Micro-Light-Emitting Diodes on a Strain Relaxed Template with an InGaN Decomposition Layer. *Crystals* **2022**, *12* (5), 721.

(11) Chan, P.; Rienzi, V.; Lim, N.; Chang, H.-M.; Gordon, M.; DenBaars, S. P.; Nakamura, S. Demonstration of Relaxed InGaN-Based Red LEDs Grown with High Active Region Temperature. *Appl. Phys. Express* **2021**, *14* (10), 101002.

(12) Pasayat, S. S.; Gupta, C.; Wong, M. S.; Wang, Y.; Nakamura, S.; Denbaars, S. P.; Keller, S.; Mishra, U. K. Growth of Strain-Relaxed InGaN on Micrometer-Sized Patterned Compliant GaN Pseudo-Substrates. *Appl. Phys. Lett.* **2020**, *116* (11), 111101.

(13) Pasayat, S. S.; Ley, R.; Gupta, C.; Wong, M. S.; Lynsky, C.; Wang, Y.; Gordon, M. J.; Nakamura, S.; Denbaars, S. P.; Keller, S.; Mishra, U. K. Color-Tunable < 10Mm Square InGaN Micro-LEDs on Compliant GaN-on-Porous-GaN Pseudo-Substrates. *Appl. Phys. Lett.* **2020**, *117* (6), 061105.

(14) Pasayat, S. S.; Gupta, C.; Acker-James, D.; Cohen, D. A.; DenBaars, S. P.; Nakamura, S.; Keller, S.; Mishra, U. K. Fabrication of Relaxed InGaN Pseudo-Substrates Composed of Micron-Sized Pattern Arrays with High Fill Factors Using Porous GaN. *Semicond. Sci. Technol.* **2019**, *34* (11), 115020.

(15) Wang, S.-J.; Li, N.; Park, E.-H.; Lien, S.-C.; Feng, Z. C.; Valencia, A.; Nause, J.; Ferguson, I. Metalorganic Chemical Vapor Deposition of InGaN Layers on ZnO Substrates. *J. Appl. Phys.* **2007**, *102* (10), 106105.

(16) Wang, S.-J.; Li, N.; Park, E.-H.; Feng, Z. C.; Valencia, A.; Nause, J.; Kane, M.; Summers, C.; Ferguson, I. MOCVD Growth of GaN-Based Materials on ZnO Substrates. *Phys. Status Solidi C* **2008**, *5* (6), 1736−1739.

(17) Li, N.; Wang, S.-J.; Huang, C.-L.; Feng, Z. C.; Valencia, A.; Nause, J.; Summers, C.; Ferguson, I. Effect of an Al2O3 Transition Layer on InGaN on ZnO Substrates by Organometallic Vapor-Phase Epitaxy. *J. Cryst. Growth* **2008**, *310* (23), 4908−4912.

(18) Lei, Y.; Xu, J.; Zhu, K.; He, M.; Zhou, J.; Gao, Y.; Zhang, L.; Chen, Y. A GaN-Based LED With Perpendicular Structure Fabricated on a ZnO Substrate by MOCVD. *J. Dispersion Technol.* **2013**, *9* (5), 377−381.

(19) Ozaki, T.; Funato, M.; Kawakami, Y. Red-Emitting $In_x Ga_{1-x} N/In_y Ga_{1-y} N$ Quantum Wells Grown on Lattice-Matched $In_y Ga_{1-y} N/ScAlMgO_4$ (0001) Templates. *Appl. Phys. Express* **2019**, *12* (1), 011007.

(20) Ozaki, T.; Takagi, Y.; Nishinaka, J.; Funato, M.; Kawakami, Y. Metalorganic Vapor Phase Epitaxy of GaN and Lattice-Matched InGaN on $ScAlMgO_4$ (0001) Substrates. *Appl. Phys. Express* **2014**, *7* (9), 091001.

(21) Ozaki, T.; Funato, M.; Kawakami, Y. InGaN-Based Visible Light-Emitting Diodes on ScAlMgO4(0001) Substrates. *Appl. Phys. Express* **2015**, *8* (6), 062101.

(22) Takahashi, R.; Fujiki, R.; Hozo, K.; Hiramatsu, R.; Matsukura, M.; Kojima, T.; Han, D.-P.; Iwaya, M.; Takeuchi, T.; Kamiyama, S. Improvement of 650-Nm Red-Emitting GaIn0.17N/GaIn0.38N Multiple Quantum Wells on ScAlMgO4 (0001) Substrate by Suppressing Impurity Diffusion/Penetration. *Appl. Phys. Lett.* **2022**, *120* (14), 142102.

(23) *ScAlMgO4 (SAM) Substrate for GaN Epitaxy*. https://www.msesupplies.com/products/scalmgo-sub-4-sub-magnesium-aluminate-scandium-oxide-sam-substrate-for-gan-epitaxy?variant=39854734245946. (accessed 28 January 2024).

(24) Wang, G.; Li, Y.; Kirch, J.; Han, Y.; Chen, J.; Marks, S.; Mukhopadhyay, S.; Liu, R.; Liu, C.; Evans, P. G.; Pasayat, S. S. MOCVD of InGaN on ScAlMgO4 on Al2O3 Substrates with Improved Surface Morphology and Crystallinity. *Crystals* **2023**, *13* (3), 446.

(25) Chen, Y.; Zuo, P.; Guan, Y.; Yusuf, M. H.; Babcock, S. E.; Kuech, T. F.; Evans, P. G. Reduction of Interface Reactions in the Low-Temperature Solid-Phase Epitaxy of ScAlMgO4 on Al2O3(0001). *Cryst. Growth Des.* **2020**, *20* (9), 6001−6007.

(26) Pantzas, K.; El Gmili, Y.; Dickerson, J.; Gautier, S.; Largeau, L.; Mauguin, O.; Patriarche, G.; Suresh, S.; Moudakir, T.; Bishop, C.; Ahaitouf, A.; Rivera, T.; Tanguy, C.; Voss, P. L.; Ougazzaden, A. Semibulk InGaN: A Novel Approach for Thick, Single Phase, Epitaxial InGaN Layers Grown by MOVPE. *J. Cryst. Growth* **2013**, *370*, 57−62.

(27) White, R. C.; Khoury, M.; Wu, F.; Keller, S.; Rozhavskaia, M.; Sotta, D.; Nakamura, S.; DenBaars, S. P. MOCVD Growth of Thick V-Pit-Free InGaN Films on Semi-Relaxed InGaN Substrates. *Semicond. Sci. Technol.* **2021**, *36* (1), 015011.

(28) Ahmed, N. M.; Sabah, F. A.; Abdulgafour, H. I.; Alsadig, A.; Sulieman, A.; Alkhoaryef, M. The Effect of Post Annealing Temperature on Grain Size of Indium-Tin-Oxide for Optical and Electrical Properties Improvement. *Results Phys.* **2019**, *13*, 102159.

(29) Sun, R.; Zhang, H.-Y.; Wang, G.-G.; Han, J.-C.; Wang, X.-Z.; Kuang, X.-P.; Cui, L.; Jin, L.; Tian, J.-L. Influence of Annealing Atmosphere on the Structure, Morphology and Transmittance of N-Incorporated Ga2O3 Films. *Superlattices Microstruct.* **2013**, *60*, 257−262.
(30) Makeswaran, N.; Battu, A. K.; Deemer, E.; Ramana, C. V. Crystal Growth and Structure−Property Optimization of Thermally Annealed Nanocrystalline Ga2O3 Films. *Cryst. Growth Des.* **2020**, *20* (5), 2893−2903.
(31) Zhang, X.; Jiang, D.; Zhao, M.; Zhang, H.; Li, M.; Xing, M.; Han, J.; Romanov, A. E. The Effect of Annealing Temperature on Ga $_2$ O $_3$ Film Properties. *J. Phys.: Conf. Ser.* **2021**, *1965* (1), 012066.

https://doi.org/10.1021/acs.cgd.4c00990
Cryst. Growth Des. 2024, 24, 9538−9543